Mine Water and the Environment (2022) 41:640–653
https://doi.org/10.1007/s10230-022-00875-6

TECHNICAL ARTICLE

Impact of Mining Activities on Groundwater Level, Hydrochemistry, and Aquifer Parameters in a Coalfield's Overburden Aquifer

Shen Qu[1,2] · Guangcai Wang[1,2] · Zheming Shi[1,2] · Zejun Zhu[1,2] · Xianbin Wang[1,2] · Xiaomei Jin[1,2]

Received: 7 October 2021 / Accepted: 4 May 2022 / Published online: 3 June 2022

Abstract
Changes in groundwater level, hydrochemistry, and aquifer parameters were studied by following disturbances caused by tunnel excavation in a panel in the Ningtiaota coalfield, northwest China. Temporal changes of hydrochemical compositions were evaluated based on time-series hydrochemical data in three boreholes (J2, J13, and SK8). The time series of hydraulic conductivity and specific storage of aquifers were obtained using the water level response to Earth tides and long-term (from 2014 to 2019) hourly recorded water level data. The results showed that the concentrations of Ca^{2+}, HCO_3^-, and TDS in groundwater in borehole J2 decreased sharply following underground tunnel excavation and recovered after six months. Back and forth changes also occurred in the hydrochemical types (HCO_3–Ca → HCO_3–Ca–Mg → HCO_3–Ca). The excavation caused changes in hydraulic conductivity (about 2 order of magnitudes) and groundwater level (about 3.2 m), possibly by unclogging fractures. This in turn caused hydrochemical changes, such as silicate dissolution and calcite precipitation, possibly due to inflow of dilute water from neighboring aquifers. After the disturbance, the concentrations of Ca^{2+}, HCO_3^-, and TDS in groundwater gradually recovered as the aquifer and groundwater levels both tended to recover, possibly due to the reclogging of fractures. This study on the coupled evolution of hydrological processes could enhance our understanding of the effects of mining on aquifer systems.

Keywords Hydrochemical changes · Hydraulic conductivity · Earth tide · Time series

Introduction

Underground coal mining can change the structure of an overburden aquifer system, resulting in complicated hydrogeological variations (Adhikary and Guo 2015; Izadi et al. 2011; Ju et al. 2017; Zhang et al. 2016). Mining directly disturbs the hydrological characteristics of groundwater systems, including long-term groundwater level declines (Qiao et al. 2011; Shi et al. 2017), variations in aquifer parameters (Sui et al. 2011; Sun et al. 2016), and hydrochemical changes (Huang and Chen 2012; Zhang et al. 2020). These hydrochemical change can pose a threat to groundwater quality and environment (Arkoc et al. 2016; Qu et al. 2018), while the changes in groundwater level could cause the redistribution of water resources and adversely affect the eco-environment (Li et al. 2018a; Liu et al. 2017; Yin et al. 2017; Zhu et al. 2020). The changes in groundwater dynamics (groundwater level) and intrinsic properties (aquifer parameters) can also affect hydrochemistry (Booth 2007; Qu et al. 2021; Xiao et al. 2018). To support sustainable utilization of water resources and prediction of water inrush, it is important to elucidate the coupled evolution of groundwater level, aquifer parameters, and hydrochemistry associated with mining activities.

In recent years, some studies have reported the hydrochemical characteristics and evolution in coalfield (Arkoc et al. 2016; Li et al. 2019; Zhu et al. 2020). Li et al. (2018b) investigated the hydrogeochemical mechanisms and the hydraulic connection between adjacent aquifers in the Hondunzi coal mine. Huang et al. (2017) identified the main hydrochemical evolution and groundwater origins in the Ningtaiota coalfield. Using the Linhuan coal mine as an example, Yin et al. (2017) revealed the mechanism of water–rock interactions caused by 20 years of

✉ Guangcai Wang
wanggc@pku.edu.cn

1 MOE Key Laboratory of Groundwater Circulation and Environmental Evolution, China University of Geosciences, Beijing 100083, China

2 School of Water Resources and Environment, China University of Geosciences, Beijing 100083, China

mining-induced disturbance. However, previous studies have mainly focused on the hydrochemical evolution of groundwater, while the association between the mining-induced changes in hydrochemistry, groundwater level, and aquifer properties has seldom been documented.

Generally, the time series of water level and hydrochemistry can be investigated by continuous in-situ monitoring and sampling. By contrast, it is difficult to obtain such a time series for aquifer parameters. Conventional methods for determining aquifer parameters include numerical simulation, physical models, and aquifer test (Adhikary and Guo 2015; Booth 2002; Meng et al. 2016; Sui et al. 2015). However, these methods are expensive, time consuming, and unsuitable for evaluating the long-term variations of aquifer parameters. Instead, the responses of well water levels to the Earth tide and barometric pressure can be used to obtain continuous time series of aquifer parameters passively and economically (Qu et al. 2020a, b).

In this paper, the groundwater level, aquifer parameters, and hydrochemical changes were studied using monitoring data in three boreholes from 2012 to 2019 in the Ningtiaota coalfield, north Shaanxi, China. During the study period, tunnel excavation was carried out from May 2018 in Panel S1222, near a borehole. Thus, the time series of hydrochemistry, groundwater level and aquifer parameters provided us with a unique opportunity to investigate and test the specific mechanisms of mining-related changes in the coalfield.

Hydrogeological Setting and Mining Activity

The Ningtiaota coalfield is located 70 km northeast of Yulin City, Shaanxi Province, China (Fig. 1a). The study area is situated inland in northwest China and has a typical temperate semi-arid continental climate. It is cold in winter and hot in summer, with an average annual temperature of 6.8 °C. The average annual precipitation is 434.1 mm while average annual evaporation is 1712 mm (Yao and Xia 2007). The main aquifers in the study area include the Jurassic Yan'an Group sandstone aquifer (J_2y), the Jurassic Zhiluo Group (J_2z) sandstone aquifer, the Salawusu Group alluvial aquifer (Q_3s), and the Quaternary eolian aquifer (Q_4^{eol}; Li et al. 2008; Yang et al. 2015). The main coal seam being mined is the 2^{-2} coal, located in the J_2y formation. The aquitards consist of the Baode Group red clay (N_2b) and the Lishi Group loess (Q_2l) (Qu et al. 2020b). Among them, the J_2z and J_2y aquifers have good hydraulic connection because of their direct contact without significant aquitards in between (Fig. 1b). However, both have a poor hydraulic connection with the Q_4^{eol} aquifer as the N_2b and Q_2l aquitards interfere, except where "skylight" aquitards exist (Dai et al. 2019).

The area of the coalfield is about 71.2 km^2, and underground coal mines have operated here for 10 years. In this study, boreholes J2, J13, and SK8 were monitored (Fig. 1b). The J2 borehole is located above Panel S1222, which has two tunnels (for transport and air return) with a height and width of 7.2 m and 5.1 m, respectively. The tunnel excavation was carried out from May 2018 to 2019, from west to east. Boreholes J13 and SK8 are both located in the southern boundary of the study area, far from Panel S1222.

Data and Analysis

A total of 25 water samples were collected from boreholes J2, J13, and SK8 from 2012 to 2019. The groundwater level data from 2014 to 2019 for this study was obtained from continuous monitoring by pressure transducers ("Solinst" levellogger, Solinst Canada Ltd.) installed in these three boreholes. The groundwater level data before 2014 was obtained from the Mining Department of the Ningtiaota Administration. Barometric pressure was monitored using a "Solinst" barologger placed in borehole SK8.

The pH was measured in situ using a portable multiparameter monitor (Manta 2.0). Groundwater samples were analyzed in a laboratory of the China University of Geosciences (Beijing) and China Earthquake Administration. Na^+, K^+, Ca^{2+}, Mg^{2+}, SO_4^{2-}, and Cl^- were measured by ion chromatography with a precision of 1%. HCO_3^- and CO_3^{2-} were determined by potentiometric titration. In hydrochemistry, the total dissolved solids (TDS) is commonly expressed by the amount of the dried residue after the water sample is evaporated to dryness. During the process, about a half of the HCO_3^- escapes as CO_2 from water samples. Thus, the TDS was equal to the sum of the major ions concentrations subtracting a half of HCO_3^- concentration (Li 1998). These results are summarized in Table 1. The measured data were checked by the charge balance error (CBE$=\left|\frac{\sum cations-\sum anions}{\sum cations+\sum anions}\right|\times 100$), with all ions are expressed in meq/L. Generally, the CBE should be below 10% (Mao et al. 2021; Xiao et al. 2021; Xu and Wang 2016); on this basis, the testing results of all of the samples were acceptable.

Since the 1960s, based on the relationship of a well-aquifer system response to earth tide, many studies have found that the well water level of a confined aquifer could be used to measure the crustal tidal strain through groundwater microdynamics (Xu et al. 2021). The well water level will fluctuate with the water flowing in or out of the well, resulting from the expansion or compression of the aquifer induced by tidal strain. On this basis, the tidal response of the well water level could reflect the hydraulic property of confined aquifers (Eqs. 1 and 2; Roeloffs 1996). If the well water level shows abnormal changes induced by a disturbance, the tidal response of the well water level may

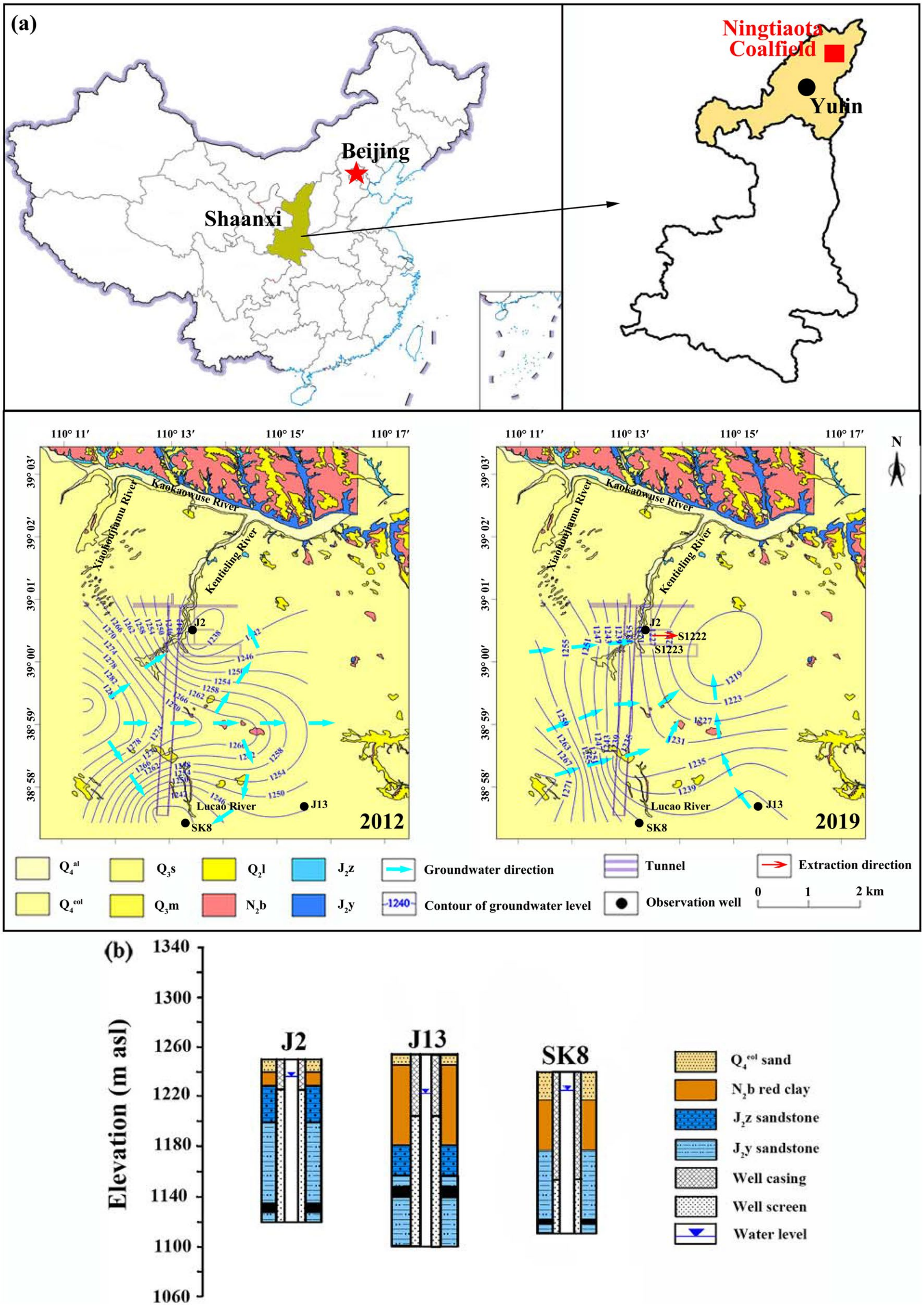

Fig. 1 **a** Geographical location and sketch map of hydrogeology of the study area and **b** cross-section maps of three observation wells

Table 1 Hydrochemical compositions of boreholes in the Ningtiaota Coalfield from 2012 to 2019

Sample date	Sample site	Ca^{2+} (mg/L)	Mg^{2+} (mg/L)	Na^{+} (mg/L)	K^{+} (mg/L)	HCO_3^{-} (mg/L)	CO_3^{2-} (mg/L)	SO_4^{2-} (mg/L)	Cl^{-} (mg/L)	TDS (mg/L)	pH	CBE (%)
2013/08	J2	27.37	6.45	7.70	1.09	135.94	0	5.68	3.08	119.35	9.01	3.49
2015/10		30.47	5.47	4.72	0.42	148.19	0	1.94	3.30	120.41	8.77	7.72
2017/09		32.57	5.83	5.26	0.56	134.77	0	1.44	3.58	116.63	8.73	0.37
2018/06		9.65	5.51	5.81	1.09	77.99	0	1.53	3.04	65.63	8.31	6.66
2018/09		24.34	5.71	6.12	0.53	103.50	0	5.95	2.69	97.09	8.49	1.97
2018/12		30.13	6.08	5.93	0.40	144.98	0	7.01	2.54	124.57	8.36	6.42
2019/04		38.63	7.19	5.94	0.39	146.44	0	7.55	2.71	135.62	7.84	3.02
2019/07		42.54	7.88	5.92	0.48	158.64	0	9.55	2.92	148.62	7.84	2.89
2019/09		43.77	7.78	6.43	0.54	152.54	0	9.07	3.20	147.06	7.73	5.92
2012/08	J13	34.10	9.70	6.60	1.00	146.40	0	7.20	3.50	135.30	8.50	3.24
2015/10		42.27	6.00	8.70	1.54	148.61	0	7.99	1.71	142.50	7.82	6.68
2018/06		31.93	6.24	7.39	1.01	150.12	0	6.62	3.73	131.99	8.27	4.66
2018/09		39.79	5.53	8.25	0.74	157.19	0	9.66	3.16	145.73	8.00	0.69
2018/12		39.86	5.50	7.93	0.69	177.19	0	9.90	2.67	155.14	8.01	6.21
2019/04		42.08	5.98	8.29	1.06	158.64	0	8.48	2.80	148.01	7.88	2.29
2019/07		41.23	5.74	8.08	0.97	164.75	0	8.05	2.69	149.13	7.99	0.48
2019/09		43.55	5.60	8.54	1.09	158.64	0	8.51	2.98	149.59	8.06	3.07
2012/08	SK8	7.54	3.26	9.58	3.34	56.93	0	6.85	4.06	63.10	-	1.69
2013/08		9.63	5.30	10.20	1.57	73.03	0	2.04	5.02	70.27	-	0.91
2018/06		4.79	5.07	12.84	1.56	75.06	0	0.75	5.48	68.02	10.03	5.28
2018/09		5.62	4.27	13.82	1.22	78.00	0	2.15	5.71	71.81	10.01	7.80
2018/12		6.24	4.23	18.42	1.24	90.25	0	3.01	5.69	83.96	10.00	6.42
2019/04		8.09	4.68	14.58	1.53	85.42	0	0.77	6.45	78.82	9.84	4.23
2019/07		6.52	4.54	14.45	1.49	73.22	0	0.92	6.26	70.79	9.64	0.89
2019/09		7.01	3.73	13.74	1.74	73.22	0	0.93	5.81	69.57	9.60	2.98

change. Consequently, the aquifer parameters derived by tidal response of the well water level (earth tide model) may also change, indicating changes in the aquifer property. In this study, the Earth tide model was used to estimate aquifer parameters, which had been proved to be effective and consistent with the results of pumping tests in the study area (Qu et al. 2020b). The same method and processes were used to estimate aquifer parameters of J2, J13, and SK8 based on the time series (groundwater level and barometric pressure) from 2014 to 2019. The aquifer parameters before 2014 cannot be estimated because the low accuracy and recording frequency of the time series provided by the Mining Department.

$$A = \left|\frac{x_0}{\varepsilon_0}\right| = \left[1 - 2\exp\left(-\frac{z}{\delta}\right)\cos\left(\frac{z}{\delta}\right) + \exp\left(-\frac{2z}{\delta}\right)\right]^{1/2}, \tag{1}$$

$$\eta = \arg\left(\frac{x_0}{\varepsilon_0}\right) = \tan^{-1}\left\{\frac{\exp\left(-\frac{z}{\delta}\right)\sin\left(\frac{z}{\delta}\right)}{1 - \exp\left(-\frac{z}{\delta}\right)\cos\left(\frac{z}{\delta}\right)}\right\}. \tag{2}$$

Here, A is the amplitude response representing the ratio between the amplitude of the water level and tidal dilation strain; η is the phase shift representing the lag time between water level oscillations and tidal dilation strain; A and η can be obtained by tidal analysis using the Baytap-G program (Tamura et al. 1991); z is the depth from the water table (m); ω is the frequency of tidal oscillation (rad/s); D is the hydraulic diffusivity (m^2/s), which equals to the division of transmissivity T (m^2/s) and storativity S. Hydraulic conductivity K (m/s) and specific storage S_s (m^{-1}) are equal to T and S divided by the aquifer thickness b (m), respectively.

Results

Variability in Groundwater Level

The groundwater level time series in boreholes J2, J13, and SK8 were analyzed (Fig. 2). J2 is located above the S1222 panel whose tunnels were excavated from west to east starting in May 2018. Boreholes J13 and SK8 are located in the southern boundary of the study area, far from Panel S1222. As shown in Fig. 2, the groundwater level in boreholes J2, J13, and SK8 show a gradual decrease before 2016. Generally, a gradual groundwater level decrease can be caused by the dewatering of formations (e.g. mine drainage; David et al. 2017). After 2016, the groundwater levels in J13 and SK8 gradually increased, but the groundwater level in J2 showed an obvious and rapid decline (about 3.2 m) from

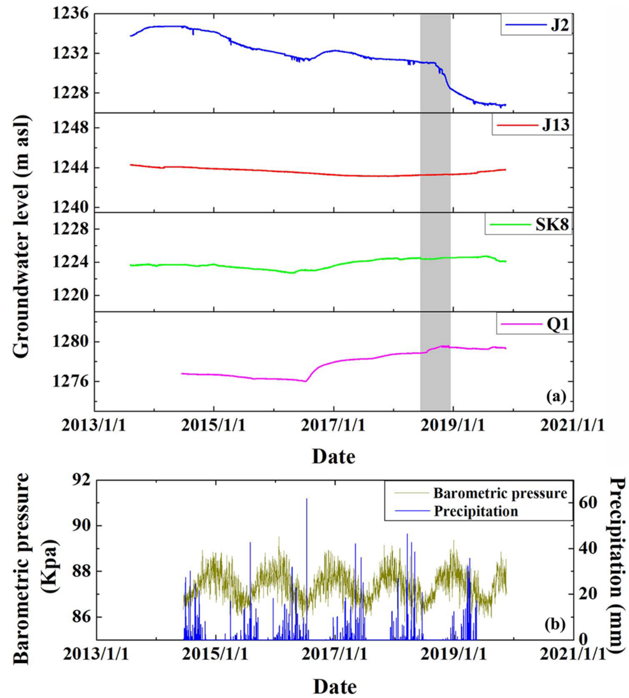

Fig. 2 The time series data of **a** groundwater level and **b** barometric pressure and precipitation

September to December, 2018, equivalent to the total groundwater level decline from 2013 to 2018 (Fig. 2a). This indicates that the groundwater level in J2 was disturbed by the nearby tunnel excavation of Panel S1222. And then, as the tunnel excavation gradually moved away from J2, the groundwater level decline began to slow down, indicating that the disturbance caused by the tunnel excavation was gradually attenuated.

Changes in Aquifer Parameters

The two-monthly mean of hydraulic conductivity K and specific storage S_s were determined with the Earth tide model (Roeloffs 1996) and calculation processes of Qu et al. (2020b). Comparing J2 with J13 and SK8 allowed us to analyze the effect of the S1222 panel mechanical disturbance on the time series of the aquifer parameters in J2. As shown in Fig. 3a, the values of K in J2, J13, and SK8 were relatively stable from 2014 to 2018, with an average value of ≈ 0.01 m/d, 0.1 m/d, and 0.01 m/d, respectively. After May 2018, the value of K in J2 increased up to 1 m/d, ≈ two order of magnitudes larger than before. The value of K recovered in about 120 days. However, the values of K in J13 and SK8 remained stable for the entire period. For the S_s time series,

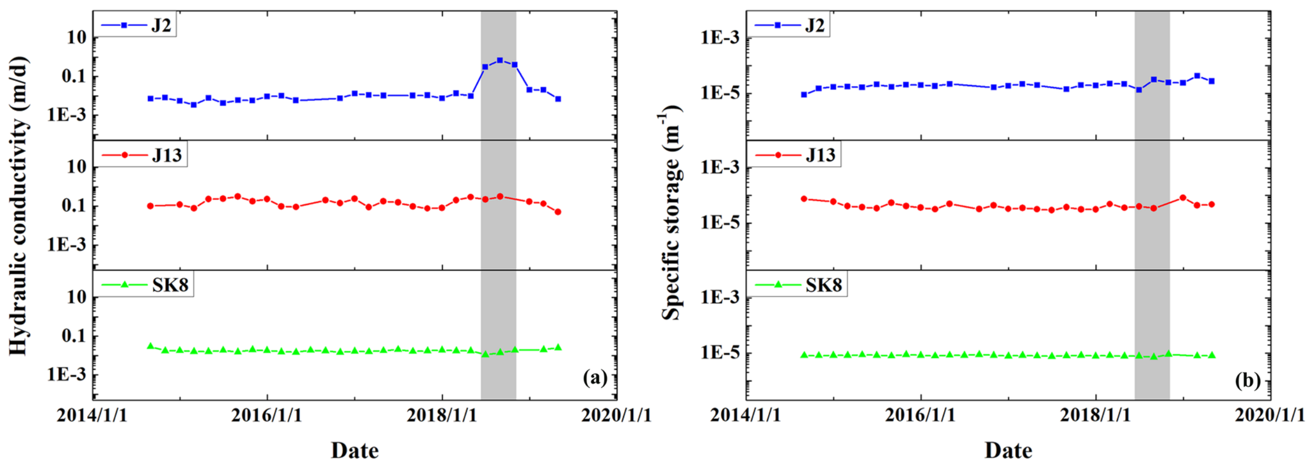

Fig. 3 Time series of **a** hydraulic conductivity K and **b** specific storage S_s. The grey area represents the period under disturbance

the values of S_s in the three boreholes remained about 1×10^{-5} m^{-1}, 1×10^{-4} m^{-1}, and 1×10^{-5} m^{-1} for the entire study period. This proved that the tunnel excavation disturbance affected the value of K but not obviously that of S_s.

Hydrochemical Variation

Evolution of Hydrochemical Type

A Piper diagram based on the major ion (K^+, Na^+, Ca^{2+}, Mg^{2+}, Cl^-, SO_4^{2-}, and HCO_3^-) time series changes from

Fig. 4 Piper diagram of water samples in three boreholes. Path (black arrow) indicates the changes under disturbance, path (orange arrow) indicates the recovery after disturbance

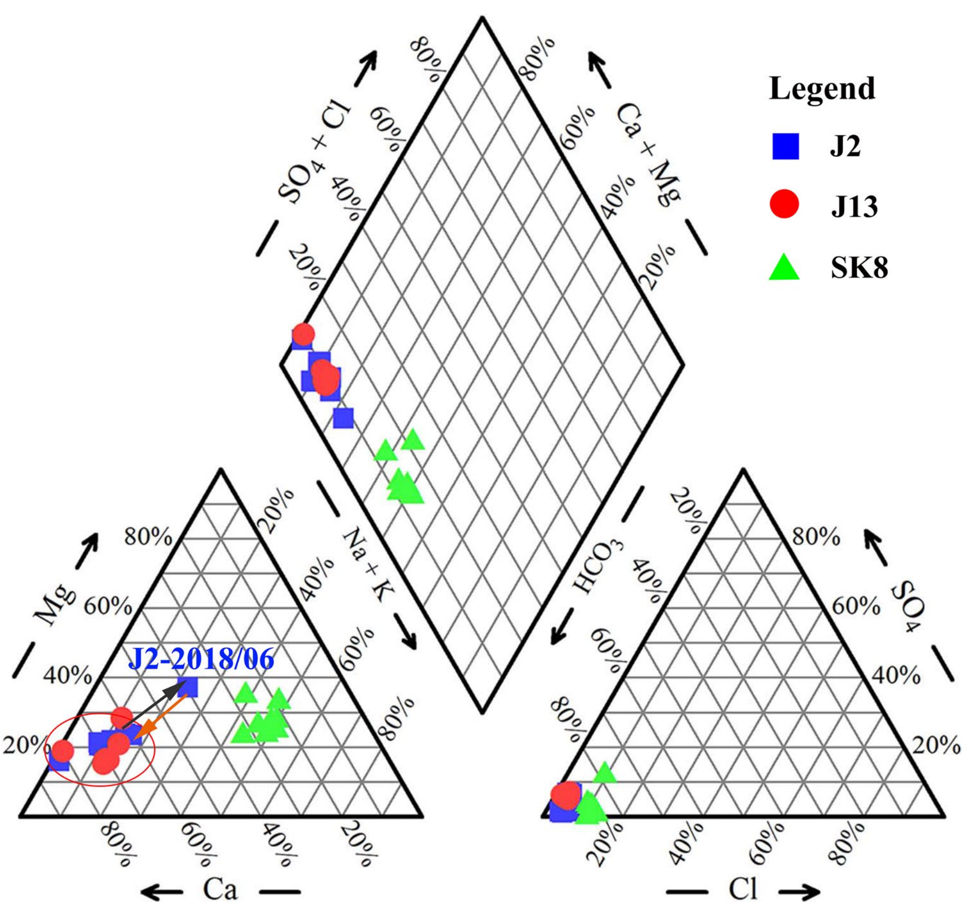

2012 to 2019 in the three boreholes was plotted (Fig. 4). As shown in the Piper diagram, the hydrochemical types in J13 and SK8 remained HCO_3–Ca and HCO_3–Na + K–Mg, and no significant changes were found for the whole study period.

Prior to June 2018, the hydrochemical type in J2 was HCO_3–Ca, consistent with J13 and different from SK8. After May 2018, borehole J2 was disturbed by tunnel excavation, its hydrochemical type changed from HCO_3–Ca to HCO_3–Ca–Mg, like SK8. And then, its hydrochemical type recovered to HCO_3–Ca as the driving face moved away (Fig. 4).

Evolution of major ions

To further explore the hydrochemical evolution, the times series for major ions and TDS in J2 were plotted to observe the changes of each component (Fig. 5). Before 2018, ion concentrations in J2 were relatively stable. After May 2018 (when tunnel excavation commenced), the concentrations of Ca^{2+} and HCO_3^- obviously decreased (Fig. 5a, b). Consequently, TDS also obviously decreased (Fig. 5c). The Ca^{2+}, HCO_3^-, and TDS concentrations recovered after 6 months as the driving face gradually moved away from J2. The Mg^{2+}, Na^+, K^+, SO_4^{2-}, and Cl^- concentrations showed little fluctuation during the study period.

To illustrate the effect of tunnel excavation on hydrochemical ions in J2, radar charts were drawn with the data from Table 1. A radar chart is a useful method for comprehensive analysis of multiple indicators, which can clearly and intuitively show the integrity and trend of indicator changes (Nguyen et al. 2015). In this study, assuming a constant rate of change for ion concentrations during some years, and using a regression analysis, the "estimated concentrations" for each ion in each well on a specific sampling day after the disturbance were obtained (Hosono and Masaki 2020). Then, the ± 2 times of standard deviation plus the estimated concentration as the upper and lower limits were used to analyze the effects of the disturbance (Nakagawa et al. 2020). If the ion concentration was above the upper limit or below the lower limit, the variation may be abnormal. The radar charts for the time series of Ca^{2+}, HCO_3^-, and TDS are shown in Fig. 6; the reference of each indicator is characterized by a red unit circle.

As shown in Fig. 6, the concentration ratios of Ca^{2+}, HCO_3^-, and TDS in J2 were close to 1 and within the range from lower limit to upper limit before 2018, indicating negligible effects from mining activity. After May 2018, a sharp decrease of Ca^{2+}, HCO_3^- and TDS occurred; the concentration ratios decreased by ≈ 72%, 43%, and 46%, respectively. Afterwards, the concentration ratios recovered, and gradually exceeded the upper limit after 2019.

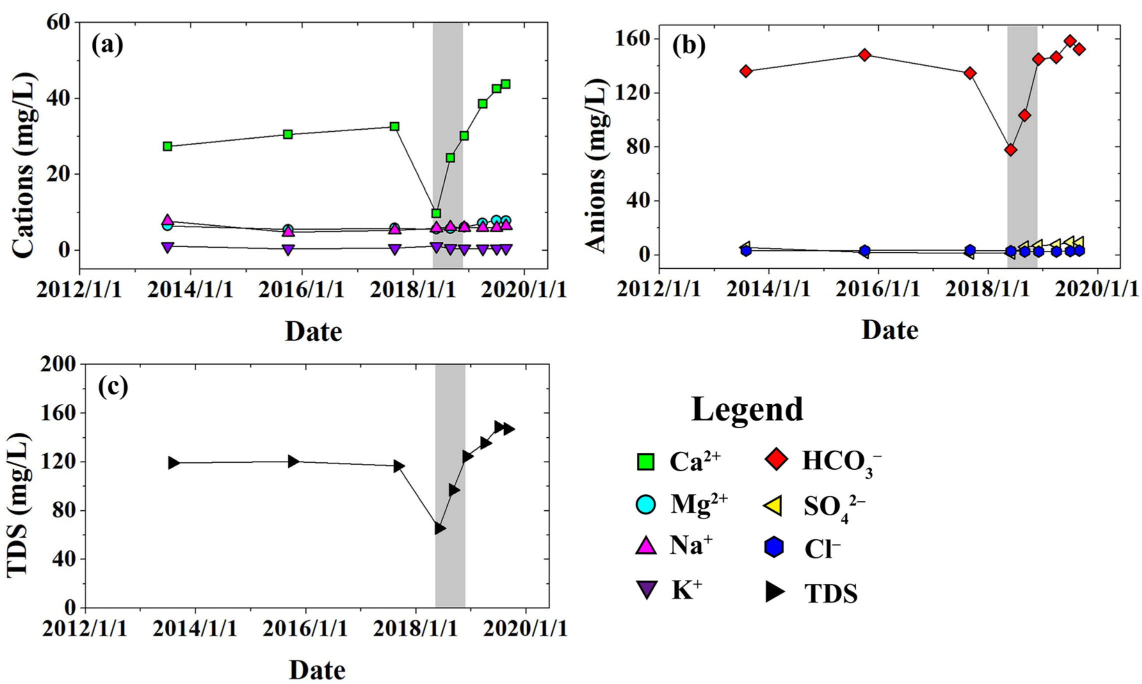

Fig. 5 Time series of major ions and TDS in the J2 borehole from 2012 to 2019. The grey area represents the period under disturbance

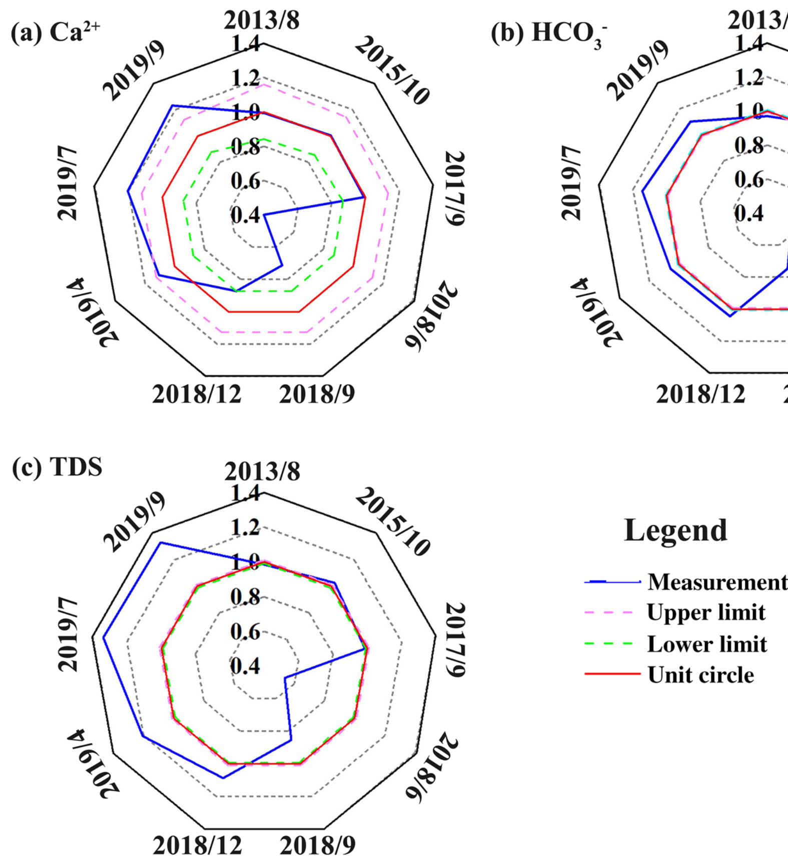

Fig. 6 Radar charts of **a** Ca^{2+}, **b** HCO_3^- and **c** TDS for J2 borehole from 2013 to 2019

Discussions

Changes in Groundwater Level and Aquifer Parameters

Prior to 2016, small changes in groundwater level and relatively constant values of aquifer parameters (K and S_s) were observed within the overburden strata. Generally, the gradual decline in groundwater level was attributed to slow depressurization and dewatering elsewhere in the coalfield (Booth 2007; David et al. 2017). After 2016, the groundwater level decline in the three boreholes slowed down, and the groundwater levels in SK8 and J13 even increased. There was no obvious correlation between the groundwater level variations in the Quaternary aquifer (Q1) and precipitation in the study area (Fig. 2), indicating that precipitation was not the main reason for the groundwater level changes. However, the Quaternary aquifer groundwater level also had an increasing trend after 2016, indicating that this trend may be a common regional characteristic in the study area rather than a phenomenon induced by mining activity. After June 2018, a rapid groundwater level decline (3.2 m) was observed in J2. This change in groundwater level was likely due to relatively rapid changes in the stress–strain state of the formation caused by the mechanical disturbance (Kim et al. 1997). In addition, the K values in J2 obviously increased after June 2018, confirming that the greater permeability was caused by the tunnel excavation. Thus, increasing the value of K can lead to a groundwater level decline.

Generally, there are two possible ways that mechanical disturbances can contribute to an increase in K: (1) the development of new fractures (Yao et al. 2011) and (2) the unclogging of clogged fractures (Liu and Manga 2009). If the disturbance leads to the development of new fractures, both K and S_s will change (Booth 2007; Ditton and Frith 2003; Mills 2012). In contrast, the unclogging of fractures would lead to an increase in K and a constant S_s (Liao et al. 2015); S_s is controlled by porosity and compressibility (Jacob 1940), which is not affected significantly by fracture unclogging. As shown in Fig. 3, a rapid increase of K was observed in J2 following the mechanical disturbance, but the S_s remained stable. Thus, the increasing K in J2 after June 2018 was likely caused by the unclogging of fractures (Fig. 7b). Although the width of the driving face (5.1 m) of tunnel excavation is much smaller than that of coal excavation (250–300 m), the width of the driving face can also damage overburden strata (Wang et al. 2009, 2016). The obviously increased K value proved that permeability of overburden strata was affected by the mechanical disturbance. After November 2018, the recovering values of K in

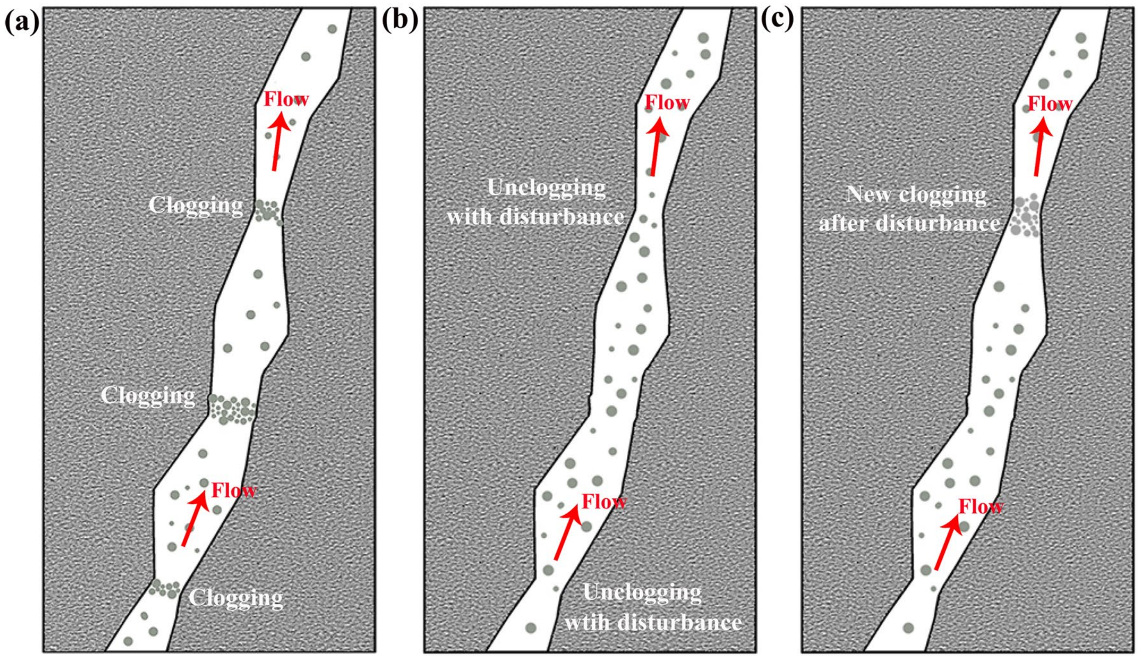

Fig. 7 Clogging and unclogging of a fracture by particles (**a** before disturbance; **b** during disturbance; **c** after disturbance)

J2 indicated reduced mechanical disturbances and the recovery of the stress field (David et al. 2017). Consequently, some previously unclogged fractures may have clogged again once the disturbance lessened (Fig. 7c). According to the hydrogeological conditions, although the main lithology in the J_2z aquifer is s medium-coarse grained sandstone, some lithology with a small grain size (e.g. sandy mudstone and siltstone) is present (Ma 2016), which provided the potential for the clogging of fractures. This is consistent with how the groundwater level decline in J2 began to slow down as the mechanical disturbance diminished.

Mechanism of Hydrochemical Changes

Natural Sources of Ions

To effectively distinguish between hydrochemical changes caused by natural and anthropogenic factors, the natural sources of hydrochemical composition should firstly be investigated (Andres and Paul 2018). The Gibbs Diagram is widely used to indicate the natural processes affecting groundwater chemistry, including precipitation, evaporation, and rock weathering, though it was initially proposed

Fig. 8 Diagrams of processes controlling the chemistry of water samples in the area: **a** TDS vs. Na/(Na + Ca), **b** TDS vs. Cl/(Cl + HCO_3)

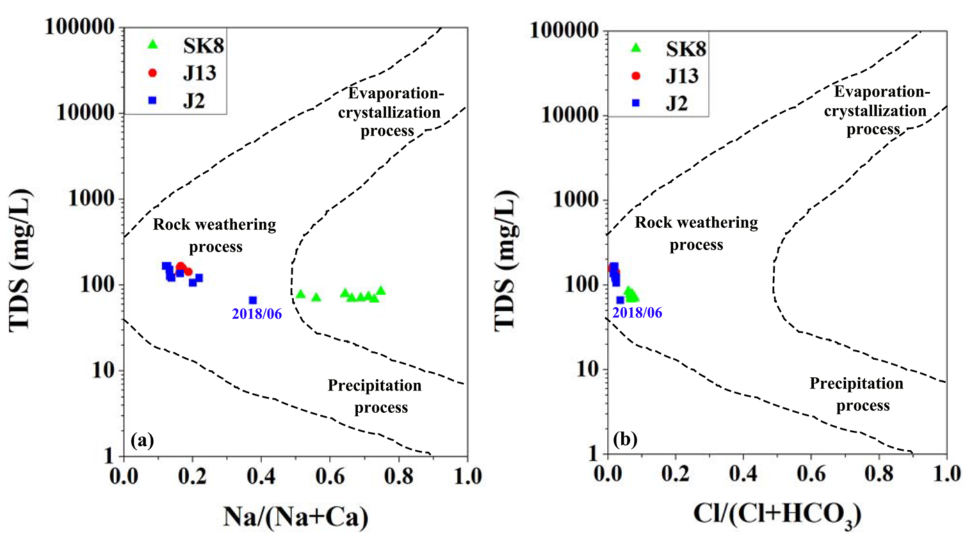

to analyze the mechanisms of river water evolution (Gibbs 1970). As shown in Fig. 8, rock weathering is the main process controlling the hydrochemical compositions of groundwater in boreholes J2, J13, and SK8. This weakens the effect of precipitation and evaporation on hydrochemical changes. It is obvious that the Na/(Na + Ca) values of SK8 are larger than that of J2 and J13 (Fig. 8a), which suggests that silicate weathering was stronger near SK8. (Banks and Frengstad 2006). By contrast, the Cl/(Cl + HCO_3) values of the three boreholes are less than the Na/(Na + Ca) values (Fig. 8), indicating that dissolution of halite is weaker than that of silicate or carbonate (Andres and Paul 2018). The scattered Na/(Na + Ca) and Cl/(Cl + HCO_3) values of J2 shifted to be like SK8, with a lower TDS in June 2018, showing the possible effect of dilution (Chen and Wang 2021). Although the TDS of J2 decreased, the Na/(Na + Ca) value obviously increased while the Cl/(Cl + HCO_3) value remained relatively stable in June 2018, which was possibly caused by silicate weathering accompanied by carbonate precipitation (Huang et al. 2017).

Hydrochemical Evolution

The possible water–rock interactions to reproduce and/or reduce Ca^{2+} and HCO_3^- in the study area are shown in Fig. 9. Generally, a positive cation exchange tends to be accompanied by a decrease of Ca^{2+} and an increase of Na^+/K^+ (Qu et al. 2021). While the Ca^{2+} concentration of groundwater in J2 significantly decreased under disturbance, no obvious increase of Na^+/K^+ was observed. The presence of cation exchange should show a linear relationship of ($Ca^{2+} + Mg^{2+} - HCO_3^- - SO_4^{2-}$) and ($Na^+ + K^+ - Cl^-$), with a slope close to − 1 (Barzegar et al. 2017; Wu et al. 2017). However, the water sample points deviated from the 1:1 line (especially J2), with poor linearity ($R^2 = 0.35$) (Fig. 10a), indicating that cation exchange was not the dominant mechanism causing the ion concentration changes in this study.

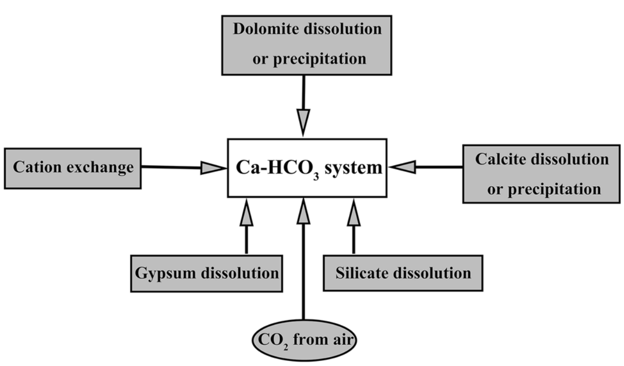

Fig. 9 Hydrochemical processes control on the Ca^{2+} and HCO_3^- of groundwater in J_2z sandstone aquifer in the Ningtiaota Coalfield

Dissolution of silicate and carbonate can also affect Ca^{2+} and HCO_3^- concentrations in aquatic systems, which can be inferred by a 1:1 ratio of HCO_3^- and Σ Cations (meq/L; Kim et al. 2005; Xu and Wang 2016). The correction was made by subtracting (Cl^-) from the sum of the major cations (Σ Cation (meq/L) = $Ca^{2+} + Mg^{2+} + Na^+ + K^+ - Cl^-$), eliminating the possible influence of NaCl or $CaCl_2$ because dissolution of these salts doesn't affect alkalinity (Garrels and Mackenzie 1967). In the study area, feldspar sandstone is the main silicate-containing mineral (Ma and Yang 2019; Qu et al. 2021). Furthermore, the groundwater is saturated/supersaturated with calcite and dolomite (Fig. 10b). Therefore, the main hydrochemical process controlling Ca^{2+} and HCO_3^- mainly include dissolution of silicate, (especially plagioclase; Eqs. 3–4; Kim 2003) and precipitation of carbonate (especially calcite; Eq. 5). This is consistent with the Gibbs diagram (Fig. 8). Although the groundwater was unsaturated with gypsum and halite, SO_4^{2-} and Cl^- changed little during the study period (Fig. 5), indicating that dissolution of gypsum and halite were not the main hydrochemical process controlling TDS.

Hydrochemical Changes Associated with Mining

As discussed above, the changes of Ca^{2+}, HCO_3^-, and TDS in J2 was not caused by precipitation or evaporation-crystallization. The mechanism of hydrochemical changes in J2 was clarified according to the above analysis of hydrochemical evolution controlling Ca^{2+} and HCO_3^-. The Ca^{2+}, HCO_3^-, and TDS concentrations showed a large decrease after the tunnel extraction in Panel S1222 and recovered afterwards. Thus, the processes had two stages:

(1) During the decline stage, from September 2017 to June 2018, the concentrations of Ca^{2+}, HCO_3^-, and TDS in J2 decreased (Fig. 5), indicating dilution. The dilution effect was inferred by the relationship between HCO_3^- and Σ cations in J2, which was close to those of SK8. After May 2018, the *K* of J2 significantly increased because as the unclogging of fractures caused the groundwater flow velocity and permeability to increase. This facilitated the groundwater level decline in J2 and the inflow of dilute water from other part of the J_2z aquifer or neighboring J_2y aquifer. Since the J_2z aquifer is characterized by feldspar sandstone and calcite was saturated/supersaturated (Fig. 10b), silicate weathering, which would be strengthened by the increased groundwater flow, could be the dominant source of Ca^{2+} (Eqs. 3–4), inducing the precipitation of the calcite (Eq. 5). The reason is that the large decline of groundwater level could have changed the hydrochemical environment from reduction to oxidation (Liu et al. 2017; Qu et al. 2018). Comparing groundwater level contours in 2012 and 2019 (Fig. 2), the groundwater level obviously declined in 2019, indicating that the hydrochemical environment may change

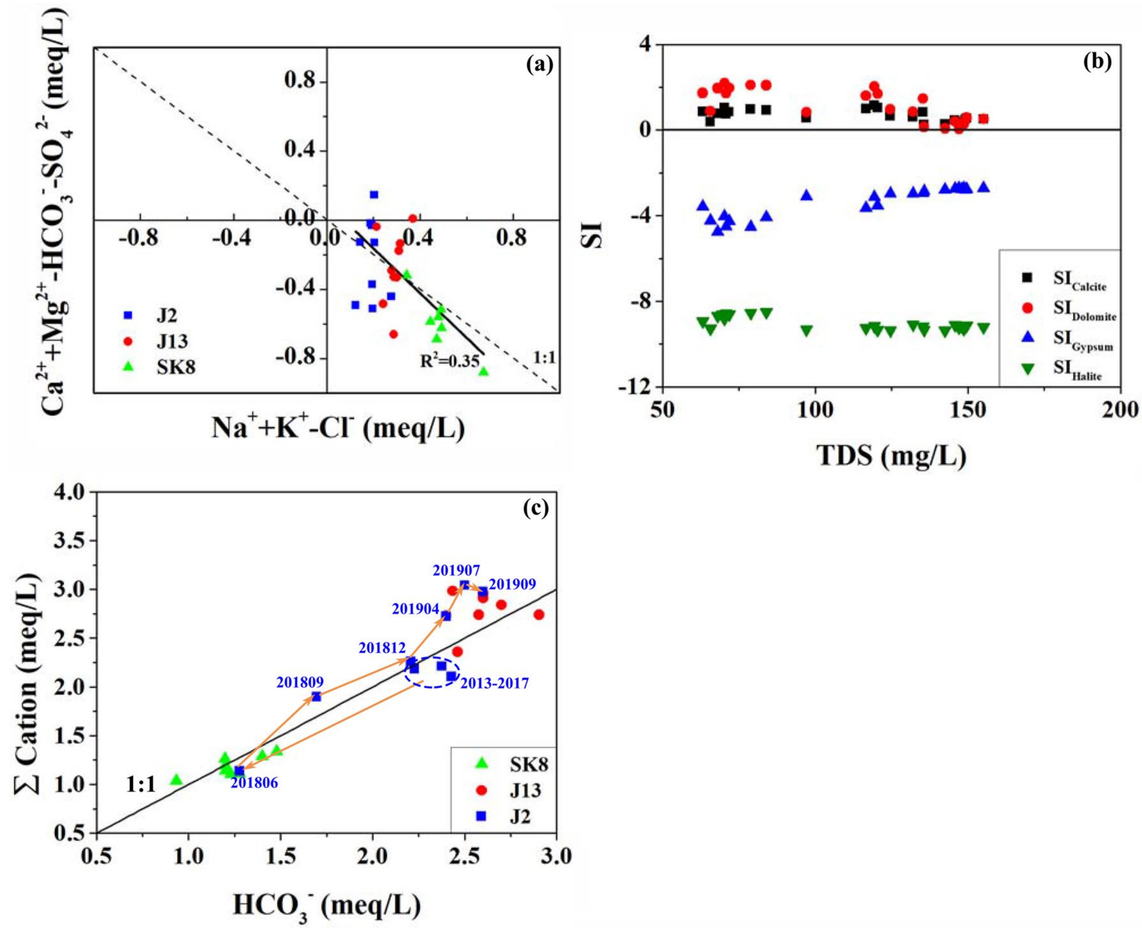

Fig. 10 Relationship between hydrochemical compositions of **a** ($Ca^{2+} + Mg^{2+} - HCO_3 - SO_4^{2-}$) and ($Na^+ + K^+ - Cl^-$); **b** equilibrium of groundwater with calcite, dolomite, gypsum and halite; and **c** relationship between corrected Σ cation and HCO_3^-

in the study area. On this basis, CO_2 could have entered the hydrochemical environment, strengthening the dissolution of anorthite because of the dissolution of CO_2 (Eqs. 3–4). And the increase of HCO_3^- from anorthite promotes the precipitation of calcite (Eq. 5). Consequently, the concentration of Ca^{2+}, HCO_3^-, and consequently TDS significantly decreased. In conclusion, the decline stage of hydrochemical changes in J2 was controlled by the inflows of dilute water and water–rock interaction.

$$CaAl_2Si_2O_8 + 3H_2O + 2CO_2 = Ca^{2+} + Al_2Si_2O_5(OH)_4 + 2HCO_3^-, \tag{3}$$

$$\begin{aligned} CaAl_2Si_2O_8 \cdot 2NaAlSi_3O_8 + 5H_2O + 3CO_2 \\ = CaCO_3 + 2Al_2Si_2O_5(OH)_4 \\ + 2Na^+ + 4SiO_2 + 2HCO_3^-, \end{aligned} \tag{4}$$

$$Ca^{2+} + HCO_3^- = CaCO_3 + H^+. \tag{5}$$

(2) During the recovery stage, after September 2018, the concentrations of Ca^{2+}, HCO_3^-, and TDS gradually returned to previous levels (Fig. 5), reflecting decayed dilution. After disturbance, these concentrations recovered and increased to a relative higher value than before mining. This may be because some previously unclogged fractures may have clogged again. This was also indicated by the recovery of *K* (Fig. 3). Meanwhile, groundwater was stored, which could have caused the increased hydrochemical compositions (Li 1998).

Conclusions

Based on continuous in-situ monitoring and sampling, and the well water level response to the Earth tide, changes of groundwater level, hydrochemistry, and aquifer parameters around borehole J2 were identified in response to tunnel excavation after May 2018. The main conclusions were that:

1. Before the tunnel excavation, the groundwater level of J2 gradually decreased without any abnormal change; the water's hydrochemical compositions and aquifer parameters also remained relatively stable.
2. After the S1222 panel tunnel excavation (after May 2018), the concentrations of groundwater Ca^{2+}, HCO_3^-, and TDS significantly decreased due to silicate dissolution and calcite precipitation associated with the inflow of dilute water; meanwhile, the groundwater level sharply decreased (about 3.2 m) and the *K* showed a large increase (about two order of magnitudes), which was caused by the unclogging of fractures.
3. Later, the concentrations of Ca^{2+}, HCO_3^-, and TDS gradually recovered as the *K* and groundwater level both recovered, as the fractures reclogged.

Acknowledgements This work was supported by the National Key Research and Development Project of China (2018YFC0406401) and the National Natural Science Foundation of China (41272269). We thank Dr. Xiang Ding, Xiangyang Liang, and Jianwen Wang from the CCTEG Xi'an Research Institute and the Ningtiaota Coal Mining Administration for their assistance in field work.

References

Adhikary DP, Guo H (2015) Modelling of longwall mining-induced strata permeability change. Rock Mech Rock Eng 48(1):345–359. https://doi.org/10.1007/s00603-014-0551-7

Andres M, Paul S (2018) Groundwater chemistry and the Gibbs diagram. Appl Geochem 97:209–212. https://doi.org/10.1016/j.apgeochem.2018.07.009

Arkoc O, Ucar S, Ozcan C (2016) Assessment of impact of coal mining on ground and surface waters in Tozakl coal field, Krklareli, northeast of Thrace, Turkey. Environ Earth Sci 75(6):1–13. https://doi.org/10.1007/s12665-015-5120-1

Banks D, Frengstad B (2006) Evolution of groundwater chemical composition by plagioclase hydrolysis in Norwegian anorthosites. Geochem Cosmochim Acta 70:1337–1355. https://doi.org/10.1016/j.gca.2005.11.025

Barzegar R, Moghaddam AA, Tziritis E, Fakhri MS, Soltani S (2017) Identification of hydrogeochemical processes and pollution sources of groundwater resources in the Marand plain, northwest of Iran. Environ Earth Sci 76:297. https://doi.org/10.1007/s12665-017-6612-y

Booth CJ (2002) The effects of longwall coal mining on overlying aquifers. Geol Soc Spec Publ 198(1):17–45. https://doi.org/10.1144/GSL.SP.2002.198.01.02

Booth CJ (2007) Confined-unconfined changes above longwall coal mining due to Increases in fracture porosity. Environ Eng Geosci 13(4):355–367. https://doi.org/10.2113/gseegeosci.13.4.355

Chen LY, Wang GC (2021) Hydrochemical changes of a spring due to the May 30, 2014 Ms 6.1 Yingjiang earthquake, southwest China. Environ Pollut 284(4):117125. https://doi.org/10.1016/j.envpol.2021.117125

Dai GL, Xue XY, Niu C, Xu K, Jiang ZQ, Xiao LL, Liu ML (2019) Disturbance characteristics of coal mining to the eco-phreatic flow field in adjacent regions. J China Coal Soc 44(3):8 (**in Chinese**)

David K, Timms WA, Barbour SL, Mitra R (2017) Tracking changes in the specific storage of overburden rock during longwall coal mining. J Hydrol 553:304–320. https://doi.org/10.1016/j.jhydrol.2017.07.057

Ditton S, Frith R (2003) Review of Industry Subsidence Data in Relation to the Influence of Overburden Lithology on Subsidence and an Initial Assessment of a Sub-Surface Fracturing Model for Groundwater Analysis. ACARP Project number 10023.

Garrels RM, Mackenzie FT (1967) Origin of the chemical compositions of some springs and lakes. Adv Chem 67(10):222–242. https://doi.org/10.1021/ba-1967-0067.ch010

Gibbs RJ (1970) Mechanisms controlling world water chemistry. Science 170(3962):1088–1090. https://doi.org/10.1126/science.170.3962.1088

Hosono T, Masaki Y (2020) Post-seismic hydrochemical changes in regional groundwater flow systems in response to the 2016 Mw7.0 Kumamoto earthquake. J Hydrol 580:124340. https://doi.org/10.1016/j.jhydrol.2019.124340

Huang PH, Chen J (2012) Recharge sources and hydrogeochemical evolution of groundwater in the coal-mining district of Jiaozuo, China. Hydrogeol J 20(4):739–754. https://doi.org/10.1007/s10040-012-0836-4

Huang XJ, Wang GC, Liang XY, Cui LF, Ma L, Xu QY (2017) Hydrochemical and stable isotope (δD and $\delta^{18}O$) characteristics of groundwater and hydrogeochemical processes in the Ningtiaota coalfield, northwest China. Mine Water Environ 37(1):119–136. https://doi.org/10.1007/s10230-017-0477-x

Izadi G, Wang SG, Elsworth D, Liu JS, Wu Y, Pone D (2011) Permeability evolution of fluid-infiltrated coal containing discrete fractures. Int J Coal Geol 85(2):202–211. https://doi.org/10.1016/j.coal.2010.10.006

Jacob CE (1940) On the flow of water in an elastic artesian aquifer. Trans Am Geophys Union 21:574–586. https://doi.org/10.1029/TR021i002p00574

Ju MH, Li XH, Yao QL, Liu SY, Liang S, Wang XL (2017) Effect of sand grain size on simulated mining-induced overburden failure in physical model tests. Eng Geol 226(30):93–106. https://doi.org/10.1016/j.enggeo.2017.05.015

Kim K (2003) Long-term disturbance of ground water chemistry following well installation. Ground Water 41(6):780–789. https://doi.org/10.1111/j.1745-6584.2003.tb02419.x

Kim J, Parizek RR, Elsworth D (1997) Evaluation of fully -coupled strata deformation and groundwater flow in response to longwall mining. Int J Rock Mech Min Sci 34(8):1187–1199. https://doi.org/10.1016/s0148-9062(97)00307-0

Kim K, Rajmohan N, Kim HJ, Kim SH, Hwang GS, Yun ST, Gu B, Cho MJ, Lee SH (2005) Evaluation of geochemical processes affecting groundwater chemistry based on mass balance approach: a case study in Namwon. Korea Geochem J 39(4):357–369. https://doi.org/10.2343/geochemj.39.357

Li XL (1998) Hydrogeochemistry, 2nd edn. Atomic Energy Press, Beijing

Li ZX, Han ML, Li JT, Yu JF, Lv DW, Liu HF (2008) On the analysis of the high-resolution sequence stratigraphy and coal accumulating law of Jurassic in Ordos Basin. J Coal Sci Eng 14(1):85–91. https://doi.org/10.1007/s12404-008-0018-0

Li XX, Wu P, Han ZW, Zha XF (2018a) Effects of mining activities on evolution of water quality of karst waters in midwestern Guizhou, China: evidences from hydrochemistry and isotopic composition. Environ Sci Pollut Res 25(2):1220–1230. https://doi.org/10.1007/s11356-017-0488-y

Li PY, Wu JH, Tian R, He S, He XD, Xue CY, Zhang K (2018b) Geochemistry, hydraulic connectivity and quality appraisal of mui-tilayered groundwater in the Hongdunzi coal mine, northwest China. Mine Water Environ 37(2):222–237. https://doi.org/10.1007/s10230-017-0507-8

Li PY, Tian R, Liu R (2019) Solute geochemistry and multivariate analysis of water quality in the Guohua phosphorite mine, Guizhou Province, China. Expos Health 11:91–94. https://doi.org/10.1007/s12403-018-0277-y

Liao X, Wang CY, Liu CP (2015) Disruption of groundwater systems by earthquakes. Geophys Res Lett 42:9758–9763. https://doi.org/10.1002/2015GL066394

Liu W, Manga M (2009) Changes in permeability caused by dynamic stresses in fractured sandstone. Geophys Res Lett 36(20):287–292. https://doi.org/10.1029/2009GL039852

Liu P, Hoth N, Drebenstedt C, Sun YJ, Xu ZM (2017) Hydro-geochemical paths of multi-layer groundwater system in coal mining regions—using multivariate statistics and geochemical modeling approaches. Sci Total Environ 601–602:1–14. https://doi.org/10.1016/j.scitotenv.2017.05.146

Ma K (2016) Numerical simulation of s1224 working face dynamic water inflow in Ningtiaota coal mine. Xi'an University of Science and Technology, Xi'an (**in Chinese**)

Ma QW, Yang CG (2019) Technical characteristics of sandstone in northern Shaanxi. Constr Technol Appl 36(2):81–84 (**in Chinese**)

Mao HR, Wang GC, Rao Z, Liao F, Shi ZM, Huang XJ, Chen XL, Yang Y (2021) Deciphering spatial pattern of groundwater chemistry and nitrogen pollution in Poyang Lake Basin (eastern China) using self-organizing map and multivariate statistics. J Clean Prod 329:129697. https://doi.org/10.1016/j.jclepro.2021.129697

Meng ZP, Shi X, Li G (2016) Deformation, failure and permeability of coal-bearing strata during longwall mining. Eng Geol 208:69–80. https://doi.org/10.1016/j.enggeo.2016.04.029

Mills KW (2012) Observations of ground movements within the overburden strata above longwall panels and implications for groundwater impacts. In: Proceedings of 38th symposium on the advances in the study of the Sydney Basin, Hunter Valley

Nakagawa K, Yu ZQ, Berndtsson R, Hosono T (2020) Temporal characteristics of groundwater chemistry affected by the 2016 Kumamoto earthquake using self-organizing maps. J Hydrol 582:124519. https://doi.org/10.1016/j.jhydrol.2019.124519

Nguyen TT, Kawamura A, Tong TN, Nakagawa N, Amaguchi H, Gilbuena R (2015) Clustering spatio-seasonal hydrogeochemical data using self-organizing maps for groundwater quality assessment in the Red River Delta, Vietnam. J Hydrol 522:661–673. https://doi.org/10.1016/j.jhydrol.2015.01.023

Qiao X, Li G, Li M, Zhou J, Du J, Du C, Sun Z (2011) Influence of coal mining on regional karst groundwater system: a case study in West Mountain area of Taiyuan City, northern China. Environ Earth Sci 64(6):1525–1535. https://doi.org/10.1007/s12665-010-0586-3

Qu S, Wang GC, Shi ZM, Xu QY, Guo YY, Ma L, Sheng YZ (2018) Using stable isotopes (δD, $\delta^{18}O$, $\delta^{34}S$ and $^{87}Sr/^{86}Sr$) to identify sources of water in abandoned mines in the Fengfeng coal mining district, northern China. Hydrogeol J 26(5):1443–1453. https://doi.org/10.1007/s10040-018-1803-5

Qu S, Wang GC, Shi ZM, Zhou PP, Xu QY, Zhu ZJ (2020a) Temporal changes of hydraulic properties of overburden aquifer induced by longwall mining in Ningtiaota coalfield, northwest China. J Hydrol 582:124525. https://doi.org/10.1016/j.jhydrol.2019.124525

Qu S, Shi ZM, Wang GC, Xu QY, Zhu ZJ, Han JQ (2020b) Using water level fluctuations in response to Earth-tide and barometric pressure changes to measure the in situ hydrogeological properties of an overburden aquifer in a coalfield. Hydrogeol J 28:1465–1479. https://doi.org/10.1007/s10040-020-02134-w

Qu S, Shi ZM, Liang XY, Wang GC, Jin XM (2021) Origin and controlling factors of groundwater chemistry and quality in the Zhiluo aquifer system of northern Ordos Basin. China Environ Earth Sci 80:439. https://doi.org/10.1007/s12665-021-09735-y

Roeloffs EA (1996) Poroelastic techniques in the study of earthquake related hydrologic phenomena. Adv Geophys 37:135–195. https://doi.org/10.1016/S00652687(08)60270-8

Shi WH, Yang TH, Yu QL, Li Y, Liu HL, Zhao YC (2017) A study of water-inrush mechanisms based on geo-mechanical analysis and an in-situ groundwater investigation in the Zhongguan iron mine. China Mine Water Environ 36(3):409–417. https://doi.org/10.1007/s10230-017-0429-5

Sui WH, Liu JY, Yang SG, Chen ZS, Hu YS (2011) Hydrogeological analysis and salvage of a deep coalmine after a groundwater inrush. Environ Earth Sci 62(4):735–749. https://doi.org/10.1007/s12665-010-0562-y

Sui WH, Hang Y, Ma LX, Wu ZY, Zhou YJ, Long GQ, Wei LB (2015) Interactions of overburden failure zones due to multiple-seam mining using longwall caving. Bull Eng Geol Environ 74(3):1019–1035. https://doi.org/10.1007/s10064-014-0674-9

Sun WJ, Zhou WF, Jiao J (2016) Hydrogeological classification and water inrush accidents in China's coal mines. Mine Water Environ 35(2):214–220. https://doi.org/10.1007/s10230-015-0363-3

Tamura Y, Sato T, Ooe M, Ishiguro M (1991) A procedure for tidal analysis with a Bayesian information criterion. Geophys J Int 104(3):507–516. https://doi.org/10.1111/j.1365-246X.1991.tb05697.x

Wang ZG, Zhou HW, Xie HP (2009) Research on fractal characterization of mined crack network evolution in overburden rock stratum under deep mining. Rock Soil Mech 30(8):2403–2408 (**in Chinese**)

Wang WX, Sui WH, Faybishenko B, Stringfellow WT (2016) Permeability variations within mining-induced fractured rock mass and its influence on groundwater inrush. Environ Earth Sci 75(4):326. https://doi.org/10.1007/s12665-015-5064-5

Wu J, Wang L, Wang S, Tian R, Xue C, Feng W, Li Y (2017) Spatiotemporal variation of groundwater quality in an arid area experiencing long-term paper wastewater irrigation, northwest China. Environ Earth Sci 76:460. https://doi.org/10.1007/s12665-017-6787-2

Xiao Y, Shao JL, Frape SK, Cui YL, Dang XY, Wang SB, Ji YH (2018) Groundwater origin, flow regime and geochemical evolution in arid endorheic watersheds: a case study from the Qaidam Basin, northwestern China. Hydrol Earth Syst Sci 22(8):4381–4400. https://doi.org/10.5194/hess-2017-647

Xiao Y, Hao Q, Zhang Y, Zhu Y, Yin S, Qin L, Li X (2021) Investigating sources, driving forces and potential health risks of nitrate and fluoride in groundwater of a typical alluvial fan plain. Sci Total Environ 802:149909. https://doi.org/10.1016/j.scitotenv.2021.149909

Xu B, Wang G (2016) Surface water and groundwater contaminations and the resultant hydrochemical evolution in the Yongxiu area, west of Poyang Lake. China Environ Earth Sci 75(3):1–16. https://doi.org/10.1007/s12665-015-4778-8

Xu Q, Wang G, Liang X, Qu S, Shi Z, Wang X (2021) Determination of mining-induced changes in hydrogeological parameters of overburden aquifer in a coalfield, northwest China: approaches using the water level response to Earth tides. Geofluids. https://doi.org/10.1155/2021/5516997

Yang H, Liu X, Yan X, Zhang H (2015) Discovery and reservoir forming geological characteristics of the Shenmu Gas Field in the Ordos Basin. Nat Gas Ind 35(6):1–13. https://doi.org/10.1016/j.ngib.2015.09.002

Yao JM, Xia F (2007) A study on hydrogeological condition and mining method in Ningtiaota Minefield (south limb). Shenmu-Fugu Mining Area. Coal Geol China 19(1):33-35+59 (**in Chinese**)

Yao QL, Li XH, Zhai QD (2011) Instability mechanism and technique of surrounding rock control of water-enriched roofs of coal drifts. J China Coal Soc 36(1):12–17 (**in Chinese**)

Yin XX, Chen LW, Xie WP, Xu DQ, Zeng W, Liu YX (2017) Main water–rock interactions and hydrochemical evolution in the aquifers under the mining-induced disturbance in a mining district. Hydrogeol Eng Geol 44(5):33–39 (**in Chinese**)

Zhang Z, Zhang R, Xie H, Gao M, Xie J (2016) Mining-induced coal permeability change under different mining layouts. Rock Mech Rock Eng 49(9):3753–3768. https://doi.org/10.1007/s00603-0160979-z

Zhang HT, Xu GQ, Zhan HB, Chen XQ, Liu MC, Wang MH (2020) Identification of hydrogeochemical processes and transport paths of a multi-aquifer system in closed mining regions. J Hydrol 589(2):125344. https://doi.org/10.1016/j.jhydrol.2020.125344

Zhu G, Wu X, Ge JP, Liu F, Zhao WG, Wu C (2020) Influence of mining activities on groundwater hydrochemistry and heavy metal migration using a self-organizing map (SOM). J Clean Prod 257:120664. https://doi.org/10.1016/j.jclepro.2020.120664